batteries

MDPI

Article

Integrated Machine Learning Framework Combining Electrical Cycling and Material Features for Supercapacitor Health Forecasting

Mojtaba Khakpour Komarsofla [1,2], Kavian Khosravinia [1,3] and Amirkianoosh Kiani [1,2,*]

[1] Silicon Hall: Micro/Nano Manufacturing Facility, Ontario Tech University, Oshawa, ON L1G 0C5, Canada; mojtaba.khakpourkomarsofla@ontariotechu.net (M.K.K.)
[2] Department of Mechanical and Manufacturing Engineering, Ontario Tech University, Oshawa, ON L1G 0C5, Canada
[3] PowerCo Canada Inc., Volkswagen Group, St. Thomas, ON N5P 1E2, Canada
* Correspondence: amirkianoosh.kiani@ontariotechu.ca

Abstract

The ability to predict capacity retention is critical for ensuring the long-term reliability of supercapacitors in energy storage systems. This study presents a comprehensive machine learning framework that integrates both electrical cycling data and experimentally derived material and structural features to forecast the degradation behavior of commercial supercapacitors. A total of seven supercapacitor samples were tested under various current and voltage conditions, resulting in over 70,000 charge–discharge cycles across three case studies. In addition to electrical measurements, detailed physical and material characterizations were performed, including electrode dimension analysis, Scanning Electron Microscopy (SEM), Energy Dispersive X-ray Spectroscopy (EDS), and Thermogravimetric Analysis (TGA). Three machine learning models, Linear Regression (LR), Random Forest (RF), and Multi-Layer Perceptron (MLP), were trained using both cycler-only and combined cycler + material features. Results show that incorporating material features consistently improved prediction accuracy across all models. The MLP model exhibited the highest performance, achieving an R^2 of 0.976 on the training set and 0.941 on unseen data. Feature importance analysis confirmed that material descriptors such as porosity, thermal stability, and electrode thickness significantly contributed to model performance. This study demonstrates that combining electrical and material data offers a more holistic and physically informed approach to supercapacitor health prediction. The framework developed here provides a practical foundation for accurate and robust lifetime forecasting of commercial energy storage devices, highlighting the critical role of material-level insights in enhancing model generalization and reliability.

Keywords: supercapacitor degradation; machine learning; material characterization; lifetime prediction; energy storage systems

Academic Editor: Alessandro Lampasi

Received: 27 May 2025
Revised: 24 June 2025
Accepted: 11 July 2025
Published: 14 July 2025

Citation: Khakpour Komarsofla, M.; Khosravinia, K.; Kiani, A. Integrated Machine Learning Framework Combining Electrical Cycling and Material Features for Supercapacitor Health Forecasting. *Batteries* **2025**, *11*, 264. https://doi.org/10.3390/batteries11070264

1. Introduction

Supercapacitors have become increasingly important in modern energy storage due to their ability to deliver high power density, rapid charge–discharge capability, and exceptional cycle life, often surpassing hundreds of thousands of cycles [1]. As global energy demands rise and fossil fuel reliance decreases, supercapacitors offer a critical solution for supporting renewable energy systems and electrified transportation. Their fast

response time and operational reliability make them ideal for applications such as hybrid electric vehicles, backup power systems, and load leveling in wind or solar installations [2]. Supercapacitors effectively bridge the gap between conventional capacitors and batteries, combining the high energy density of the latter with the fast kinetics and longevity of the former [3].

The performance of supercapacitors is significantly influenced by the materials used for electrodes and electrolytes. Carbon-based materials, including activated carbon, carbon nanotubes (CNTs), and graphene, are favored for their high surface area, electrical conductivity, and structural versatility [1]. Additionally, the growing interest in natural and biomass-derived carbons offers a sustainable and cost-effective alternative, aligning with environmental and manufacturing goals [4]. Meanwhile, the choice of electrolyte, whether aqueous or organic, plays a key role in defining voltage stability and energy capacity [5]. As highlighted in recent studies, material innovations continue to push the limits of energy and power density, enabling supercapacitors to serve as indispensable components in next-generation energy storage systems [2].

Capacitance, as a core performance metric, reflects the supercapacitor's ability to store and deliver electrical energy. It is influenced by the surface area and porosity of the electrode material, the dielectric properties of the electrolyte, and the physical configuration of the cell [6,7]. Traditional models relate capacitance to electrode surface area and charge separation distance. Yet, modern studies highlight the complexity of these relationships, particularly in porous carbon materials used for electrochemical double-layer capacitors (EDLCs) [8]. These insights necessitate refined characterization approaches that more accurately reflect real electrochemical environments.

Maintaining capacitance over time, known as capacity retention, is equally critical for reliable device operation. Supercapacitors degrade due to physical and chemical changes in electrodes and electrolytes during repeated cycling and under thermal and voltage stress [9]. High voltages and elevated temperatures accelerate these aging processes, ultimately limiting the useful lifespan of supercapacitors [10]. To address these challenges, recent advancements have explored strategies such as integrating nanostructured materials, hybrid EDLC/pseudocapacitive architectures, and gel polymer electrolytes with ceramic fillers to boost both capacitance and retention [10,11]. Innovations such as metal–organic frameworks (MOFs) with high porosity and redox-active sites have shown promise in boosting energy and power density [12], while hierarchical structuring of spaced TiO_2 nanotube arrays—decorated with nanoparticles and treated via selective nitridation—has enabled the development of binder-free electrodes with enhanced electronic conductivity, high-rate performance, and superior cycling stability [13]. Furthermore, studies comparing capacitance measurement methods reveal that accurate characterization depends not only on the method used but also on voltage and discharge conditions, which impact capacity estimation and health monitoring in practical applications [7]. Together, these developments highlight the central role of capacity and its retention in determining supercapacitor viability for emerging energy storage applications. While these advances in material design have significantly improved performance, modeling and predicting long-term behavior remain challenging. This is where data-driven approaches, particularly machine learning, offer powerful tools to complement experimental insights.

In parallel with these material advances, machine learning (ML) has emerged as a powerful approach to model and predict supercapacitor behavior, offering significant advantages over traditional empirical methods. While conventional models rely heavily on labor-intensive experimentation and simplified relationships, ML techniques, especially artificial neural networks (ANNs), can leverage large, complex datasets to provide accurate predictions of capacitance and degradation trends [14–16]. These models incorporate a

range of physical and chemical descriptors, such as specific surface area, pore size, and heteroatom doping, to capture the nuanced interplay of factors that drive supercapacitor performance [17]. Extending beyond static performance prediction, recent studies have demonstrated the capability of ML to forecast dynamic behaviors such as cycle life and long-term degradation [18,19]. In addition to cycle life and degradation modeling, researchers have explored hybrid approaches that combine ML with optimization algorithms to enhance electrode fabrication [20,21]. For instance, Khosravinia and Kiani applied an ANN model coupled with simulated annealing to identify optimal laser processing parameters for fabricating pseudo-capacitor electrodes with improved specific capacitance and low impedance [22]. Such integration of ML in experimental workflows accelerates material discovery and design. Moreover, Mishra et al. introduced a large-scale database of carbon electrode properties and demonstrated the ability of extreme gradient boosting to identify key physicochemical predictors of capacitance, including nitrogen doping and potential window [23]. Collectively, these studies highlight the transformative role of machine learning in guiding data-driven design, performance prediction, and lifecycle management of next-generation supercapacitors [24].

While previous studies have successfully applied machine learning to predict supercapacitor performance, most rely heavily on simulated or literature-based datasets and lack the experimental rigor seen in real-world cycling tests. For instance, Zhu et al. [14] and Reddy et al. [15] built ANN models using data extracted from hundreds of published sources to predict specific capacitance based on features such as specific surface area, pore size, and nitrogen doping levels. Similarly, Tawfik et al. [17] combined electrochemical and structural parameters in ANN and SVMR models, though their dataset was also derived from prior publications and focused on specific capacitance prediction. These studies, while valuable in establishing the role of physiochemical descriptors, often suffer from inconsistency in test conditions and do not reflect long-term degradation under controlled experimental setups. Ren et al. [18] advanced this area by focusing on early-cycle life prediction using ANN, but their work was based on limited early-cycle data and did not integrate detailed material characterizations. In contrast, the present study contributes a novel framework grounded in over 70,000 lab-generated charge–discharge cycles across three distinct electrical conditions, coupled with SEM, EDS, TGA, and electrode dimension analyses. This combination of long-term experimental evidence and detailed material profiling enables more accurate and generalizable models for forecasting capacity retention, highlighting our framework's unique capability to bridge electrochemical and physical material behavior in commercial supercapacitors. In addition to electrical cycling data, the study incorporated a comprehensive set of physical and material characterization tests. These included disassembly and dimensional analysis of electrodes, surface morphology examination via Scanning Electron Microscopy (SEM), elemental composition analysis using Energy Dispersive X-ray Spectroscopy (EDS), and thermal stability evaluation through Thermogravimetric Analysis (TGA). The resulting dataset captured structural, compositional, and thermal attributes of the electrode materials alongside temporal electrochemical behavior. To the best of the authors' knowledge, this is among the first studies to integrate such detailed material-level insights with supervised machine learning for capacity retention prediction in commercial supercapacitors. By assembling a structured, multimodal dataset derived from extensive laboratory testing, the study establishes a foundation for more physically grounded and data-driven modeling of supercapacitor performance and degradation.

2. Methodology

The following methodology section outlines the sequential procedure followed in this study. It is structured into five key subsections: Sections 2.1–2.5. This segmentation

is intended to provide a logical flow and enhance readability by clearly delineating each stage of the research process.

2.1. Supercapacitor Selection

This study employed a set of seven commercial supercapacitors to evaluate capacity retention and train predictive machine learning models. Five of these supercapacitors (SC1 to SC5) were used for model training, and two additional samples (U1 and U2) were used for validation. Each supercapacitor shared the same nominal capacitance of 50 F but differed in electrical properties and physical characteristics such as equivalent series resistance (ESR), energy density, power density, and mass. Table 1 presents detailed specifications, including ESR, energy and power density, and weight. These variations provided a diverse dataset to investigate the effect of material characteristics on performance degradation.

Table 1. Specifications of commercial supercapacitors.

SC_ID	Capacitance (F)	ESR (mΩ)	Energy Density (Wh/kg)	Power Density (kW/kg)	Weight (mg)
SC1	50	22	3.616	2.84	13,455.8
SC2	50	15	3.365	3.89	13,297.3
SC3	50	10	3.5	N.A.	10,759.1
SC4	50	10	N.A.	N.A.	12,312.4
SC5	50	20	4.5	8.13	11,587.7
U1	50	10	4.1	4.4	11,929.5
U2	50	25	3.061	1.058	13,349.6

Note: "N.A." indicates that the corresponding energy or power density data were not available from the manufacturer.

2.2. Physical Measurement and Material Characterization Tests

To quantify structural attributes relevant to supercapacitor performance, each device was carefully disassembled, and the electrodes were examined individually. Using high-precision digital measurement tools, the length, width, thickness, and weight of both the anode and cathode components were recorded. These measurements enabled the calculation of surface area, electrode density, and mass distribution factors that influence the capacity retention of the supercapacitors. This physical dataset was later integrated as input features for machine learning models to evaluate their predictive influence.

Following the physical measurements, material characterization tests were conducted to further explore the compositional and structural aspects of the electrode materials. Scanning Electron Microscopy (SEM) (Hitachi FlexSEM 1000) was used to visualize surface morphology at magnifications of 1000× and 5000×. These images provided qualitative insights into texture and porosity and were quantitatively analyzed using ImageJ software (Fiji Version). The software applied thresholding techniques to high-magnification SEM images to estimate surface porosity by distinguishing solid and void areas.

In conjunction with SEM, Energy Dispersive X-ray Spectroscopy (EDS) was performed using an Oxford EDS analyzer to determine the elemental composition of the electrode materials. The focus was on detecting the presence and relative quantities of carbon (C) and fluorine (F), typical constituents of activated carbon and PVDF-based binders. These elemental profiles revealed variations in binder content and electrode purity that could affect electrochemical behavior.

Lastly, Thermogravimetric Analysis (TGA) was carried out using a TA Instruments Q50 system under an inert atmosphere to assess thermal stability and material decomposition patterns. The TGA curves showed multi-stage degradation processes, including initial

moisture loss, polymer binder decomposition, and carbon backbone breakdown. Key parameters such as remaining weight percentage, derivative weight, and decomposition temperature were extracted and used as predictive indicators for degradation modeling.

2.3. Cycler Test

To evaluate the long-term performance and degradation behavior of commercial supercapacitors, Constant Current Charge and Discharge (CCCD) testing was performed using a Neware battery cycler system, which had eight channels for testing supercapacitors. The test protocol aimed to simulate realistic high-cycle operating conditions by repeatedly subjecting each supercapacitor to thousands of charge–discharge cycles under controlled current and voltage parameters. A total of three CCCD testing configurations designated as CCCD1, CCCD2, and CCCD3 were defined to examine the impact of electrical stress on capacity retention and energy efficiency.

CCCD1: All five training supercapacitors (SC1–SC5) were charged and discharged at a current of 5 A and voltage of 2.6 V for 30,000 continuous cycles. This configuration served as a baseline to evaluate long-term behavior under moderate electrical stress.

CCCD2: To investigate the effect of elevated voltage on performance degradation, the current was held at 5 A, while the voltage was increased to 3.5 V. The test was conducted for 30,000 cycles.

CCCD3: In this configuration, the voltage was maintained at 3.5 V (as in CCCD2), but the current was reduced to 3 A, allowing evaluation of how lower current levels influence capacity fading over 30,000 cycles.

Throughout these tests, the cycler system recorded critical parameters such as capacity retention, charge–discharge time, and energy efficiency at each cycle. The collected data were processed and structured into a machine learning-ready format to serve as input for the capacity prediction models. This rich time-series data set captured degradation patterns under different stress conditions, enabling comprehensive model training and validation across varying operating scenarios. Detailed information regarding the CCCD test protocols, including current, voltage, test step time, and cycle count, is provided in the Supplementary Materials (Figure S2 and Table S1).

2.4. Data Combining and Modeling

2.4.1. Data Cleaning and Combining

Prior to model development, the raw data obtained from the cycler device during the CCCD tests underwent a comprehensive data cleaning process. Noisy or incomplete entries were removed, and the remaining dataset was smoothed and structured for analysis. To accurately represent the capacity degradation trend over cycles, a 6th-order polynomial regression was fitted to each cleaned dataset, as shown in the equation below. The quality of these fits was validated by a coefficient of determination (R^2) exceeding 0.97, confirming that the polynomial model reliably captured the underlying degradation behavior.

$$Y = Intercept + B_1X^1 + B_2X^2 + B_3X^3 + B_4X^4 + B_5X^5 + B_6X^6 \quad (1)$$

Following the curve fitting stage, all cleaned and processed data from the electrical cycling tests, material characterization (SEM, EDS, TGA), and physical measurements were merged into a unified dataset. This comprehensive dataset included temporal features (such as cycle index and charge–discharge time), material features (e.g., porosity, elemental composition, thermal behavior), and structural parameters (e.g., electrode thickness and weight). This integrated data set formed the foundation for training, testing, and evaluating multiple machine learning algorithms to predict the capacity retention of supercapacitors under diverse conditions.

2.4.2. Modeling with Machine Learning Algorithms

To analyze and predict supercapacitor capacity retention, three machine learning models were implemented:

Linear Regression (LR):

Linear Regression is one of the most fundamental and widely used supervised learning algorithms for modeling the relationship between a dependent variable and one or more independent variables. In simple Linear Regression, the model involves one independent variable, while in multiple Linear Regression, it incorporates several predictors. The general equations for the multiple LR are expressed as follows [25]:

$$y = a + b_1x_1 + b_2x_2 + \cdots + b_nx_n + \epsilon \quad (2)$$

where:

y = output variable

x = input variable

a = intercept of the regression line

b = slope of the plot

ϵ = the regression reminder

Random Forest (RN):

Random Forest is an ensemble machine learning algorithm that operates by constructing a multitude of decision trees during training and outputting the average (for regression) or majority vote (for classification) of their predictions. It is based on the principle of bagging (bootstrap aggregating), where each tree is trained on a randomly sampled subset of the data with replacement. For a given input vector x, the Random Forest regressor predicts the output $\hat{y}$ by averaging the outputs from B individual regression trees $h_b(x)$, each trained on a bootstrap sample of the data [26]:

$$\hat{y} = \frac{1}{B}\sum_{b=1}^{B} h_b(x) \quad (3)$$

Multilayer Perceptron (MLP):

A Multilayer Perceptron (MLP) is a class of feedforward artificial neural networks that consists of an input layer, one or more hidden layers, and an output layer. Each layer is composed of neurons (or nodes), where each neuron in each layer is connected to all neurons in the next layer. The MLP learns a mapping from inputs x $\in R^n$ to outputs $\hat{y}$ by optimizing the weights of these connections through backpropagation and gradient descent [27]. For a single hidden layer MLP, the output $\hat{y}$ can be expressed as [26]:

$$\hat{y} = f^{(2)}\left(W^{(2)}f^{(1)}\left(W^{(1)}x + b^{(1)}\right) + b^{(2)}\right) \quad (4)$$

where:

$W^{(1)}, W^{(2)}$ are the weight matrices for the first and second layers, respectively.

$b^{(1)}, b^{(2)}$ are the corresponding bias vectors.

$f^{(1)}, f^{(2)}$ are activation functions (e.g., ReLU, sigmoid, or tanh).

The dataset was structured with electrical features as input variables, and capacity retention as the target variable. Initially, the models were trained using only electrical features. Subsequently, material properties obtained from SEM, EDS, and TGA tests were incorporated as additional features to evaluate their effect on model precision and predictive performance. To evaluate the performance of the machine learning models and analyze the impact of different feature sets, four commonly used statistical metrics were employed: the coefficient of determination (R^2), Mean Absolute Error (MAE), Root Mean Squared Error (RMSE), and Pearson correlation coefficient. These metrics provide

a comprehensive assessment of model accuracy, error distribution, and linear correlation between predicted and actual values.

2.5. Validation and Generalizability

To validate the machine learning model, two additional supercapacitors were tested separately. The experimental results were compared with the predictions of the trained machine learning models to assess their accuracy and reliability in forecasting capacity retention. The comparison aimed to determine the effectiveness of integrating material properties into the prediction framework and to validate the robustness of the models. The flowchart illustrating the overall process of data collection, model training, feature integration, etc., is shown in Figure 1.

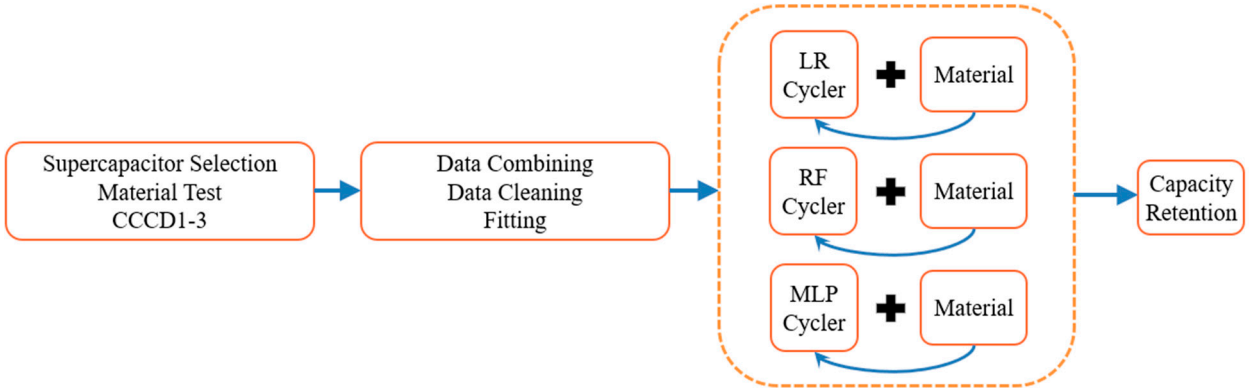

Figure 1. Overview of the experimental and modeling workflow for supercapacitor capacity retention prediction. Arrows inside the dashed box represent sequential model training first using cycler data, followed by retraining with additional material properties.

3. Results and Discussion

3.1. Physical Properties of Supercapacitors

To understand how structural attributes may influence the electrochemical performance of commercial supercapacitors, a detailed analysis of physical properties was conducted for all seven samples (SC1–SC5, U1, and U2). Each supercapacitor was disassembled, and high-precision measurements were taken for the length, width, thickness, and mass of both the anode and cathode electrodes using digital instruments. The measured values for length, width, thickness, and weight are summarized in Table 2. Where A, C, L, W, and T stand for anode, cathode, length, width, and thickness, respectively.

Table 2. Physical features of supercapacitors.

	L_C (mm)	L_A (mm)	W_C (mm)	W_A (mm)	T_C (mm)	T_A (mm)	$Weight_C$ (mg)	$Weight_A$ (mg)
SC1	403	433	30	30	0.2	0.2	2616	2778.2
SC2	365	400	32	32	0.22	0.22	2761.6	3011.4
SC3	315	321	27	27	0.23	0.23	1952.3	2075.9
SC4	492	451	32	32	0.15	0.15	2618.6	2404.6
SC5	326	358	30	30	0.17	0.17	1796.5	2316.5
U1	326	351	30	30	0.2	0.2	2065.1	2539.4
U2	403	433	32	32	0.22	0.22	2688.4	2936.1

The results revealed considerable variation across different commercial models. For instance, SC4 exhibited the largest electrode dimensions, with cathode and anode lengths measuring approximately 492 mm and 451 mm, respectively, while SC3 had the smallest

physical footprint. Thickness was relatively consistent among all samples, ranging between 0.15 mm and 0.23 mm, with SC4 again showing the thinnest electrodes. Electrode mass also varied notably, with SC2 possessing the heaviest anode and cathode pair, while SC5 was the lightest overall. These variations in geometric and mass-based features can significantly impact thermal management, ion diffusion pathways, and current distribution during operation. Consequently, they were included as predictive input features for machine learning models aimed at forecasting capacity retention.

3.2. Material Characterization

All To investigate the internal degradation mechanisms and material-level differences among the tested supercapacitors, a series of material characterization tests were conducted. These included Scanning Electron Microscopy (SEM), Energy Dispersive X-ray Spectroscopy (EDS), and Thermogravimetric Analysis (TGA), performed on both training samples (SC1–SC5) and unseen validation samples (U1, U2).

To assess the surface morphology of the electrodes after extensive cycling, SEM imaging was performed on all seven commercial supercapacitors at magnifications of $\times$5000 (Figure 2). The considered magnification ($\times$5000) offers detailed insight into microstructural features such as particle aggregation, porosity, and degradation patterns.

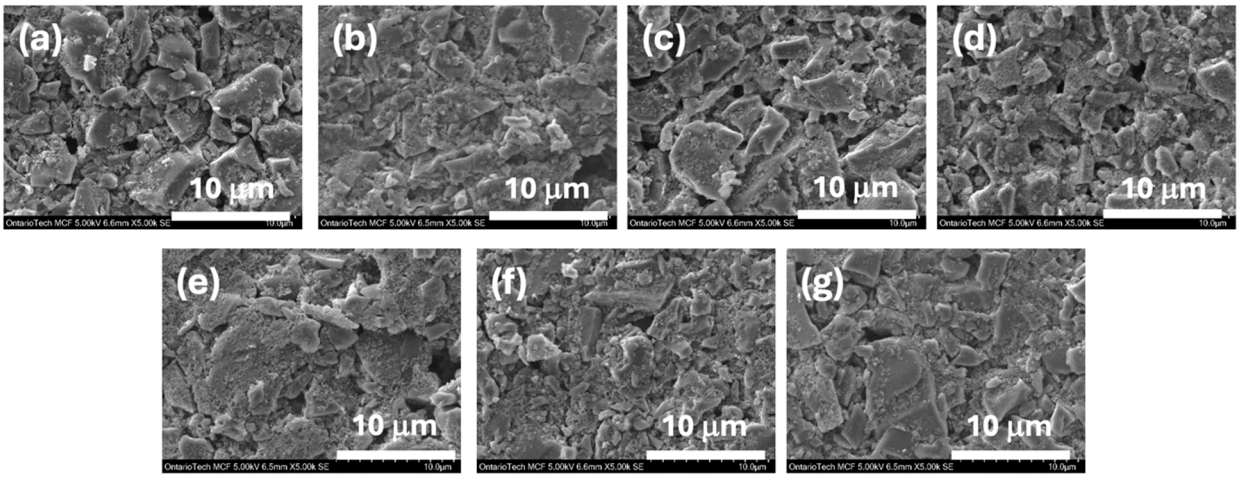

Figure 2. (**a**–**g**) SEM images of supercapacitor electrodes at 5000$\times$ for SC1-5, U1, U2 respectively.

Magnification for SC1–5, U1, U2, respectively.

Porosity was quantified using ImageJ by applying a manual thresholding method to segment pore regions from the solid matrix in the SEM images. The threshold range was set between 45 and 89 on an 8-bit grayscale scale (0–255), with red overlay used to visualize the selected pore regions. The "Raw values" and "Stack histogram" options were enabled to maintain consistent intensity interpretation. The threshold values were chosen based on visual inspection to ensure accurate segmentation of low-intensity regions corresponding to pores. Porosity was then calculated as the percentage of the thresholded (red) area relative to the total image area. A representative ImageJ thresholding figure is provided in the Supplementary Materials to illustrate the segmentation criteria in Figure S3. The resulting porosity values are presented in Figure 3, which highlights clear differences among the samples. Notably, SC3 shows the highest porosity; in contrast, SC1 has the lowest one, suggesting a denser electrode microstructure. These porosity trends are consistent with the morphological features observed in the SEM images and can significantly influence the electrochemical performance and degradation behavior of the supercapacitors.

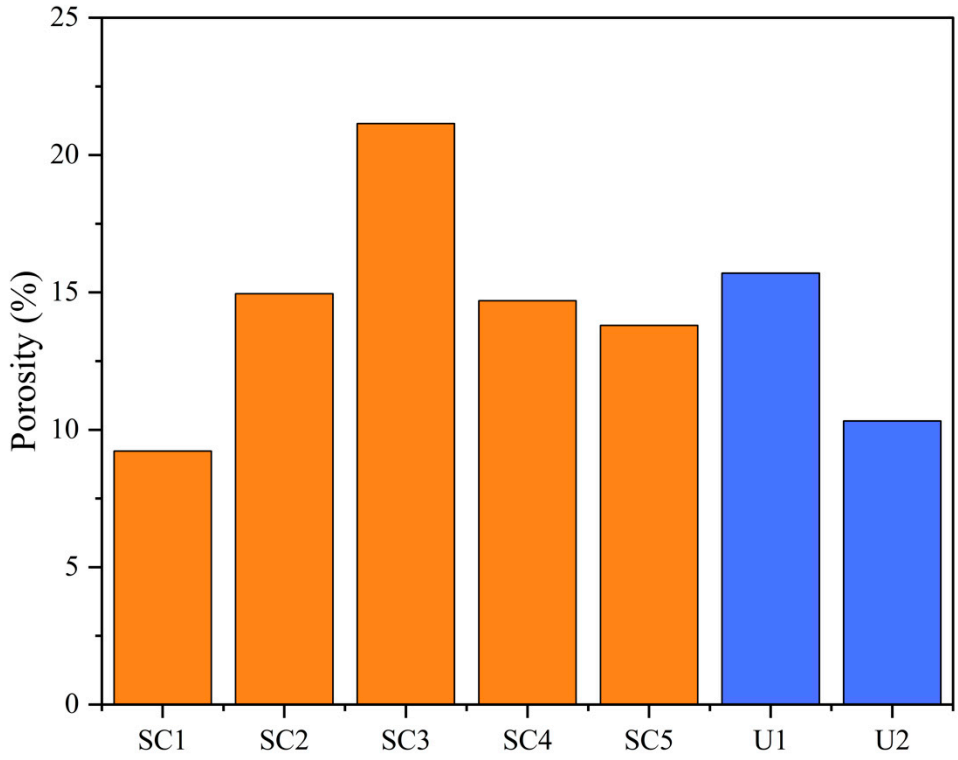

Figure 3. Porosity values for all supercapacitors.

To determine the elemental composition of the electrode materials, EDS was conducted on all five supercapacitor samples. The analysis focused on quantifying the relative atomic percentages of carbon (C) and fluorine (F), which are the primary constituents of typical activated carbon electrodes and their surface treatments. The results are illustrated in Figure 4, where the composition of each electrode is compared in terms of carbon and fluorine content. Also, detailed EDS layered images are provided in the Supplementary Materials in Figure S4.

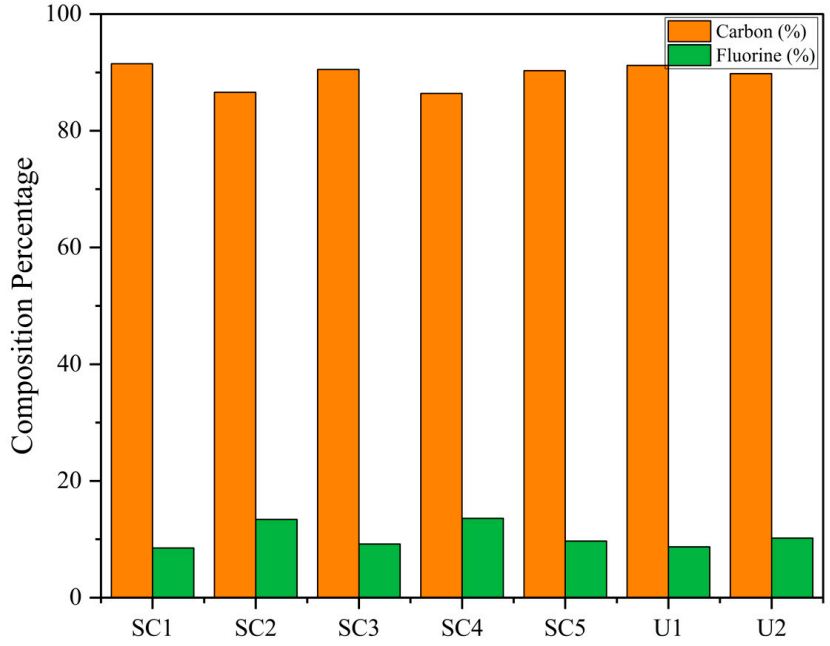

Figure 4. Elemental composition of carbon and fluorine in the electrodes.

All samples exhibited high carbon concentrations, ranging from 87% to 93%, consistent with the expectation of activated carbon-based electrodes. Fluorine levels varied between 8% and 13%, which is typically associated with the presence of PVDF (polyvinylidene fluoride) binder or surface functionalization. These elemental variations may correlate with electrochemical performance and degradation behavior. For example, higher fluorine content could enhance mechanical stability but might reduce porosity and capacitance. The EDS results thus provide critical insights into compositional differences that complement the morphological observations from SEM and the quantitative porosity analysis.

To evaluate the thermal stability and decomposition characteristics of the electrode materials, Thermogravimetric Analysis (TGA) was performed for each supercapacitor sample under an inert atmosphere. The weight loss curves as a function of temperature are shown in Figure 5.

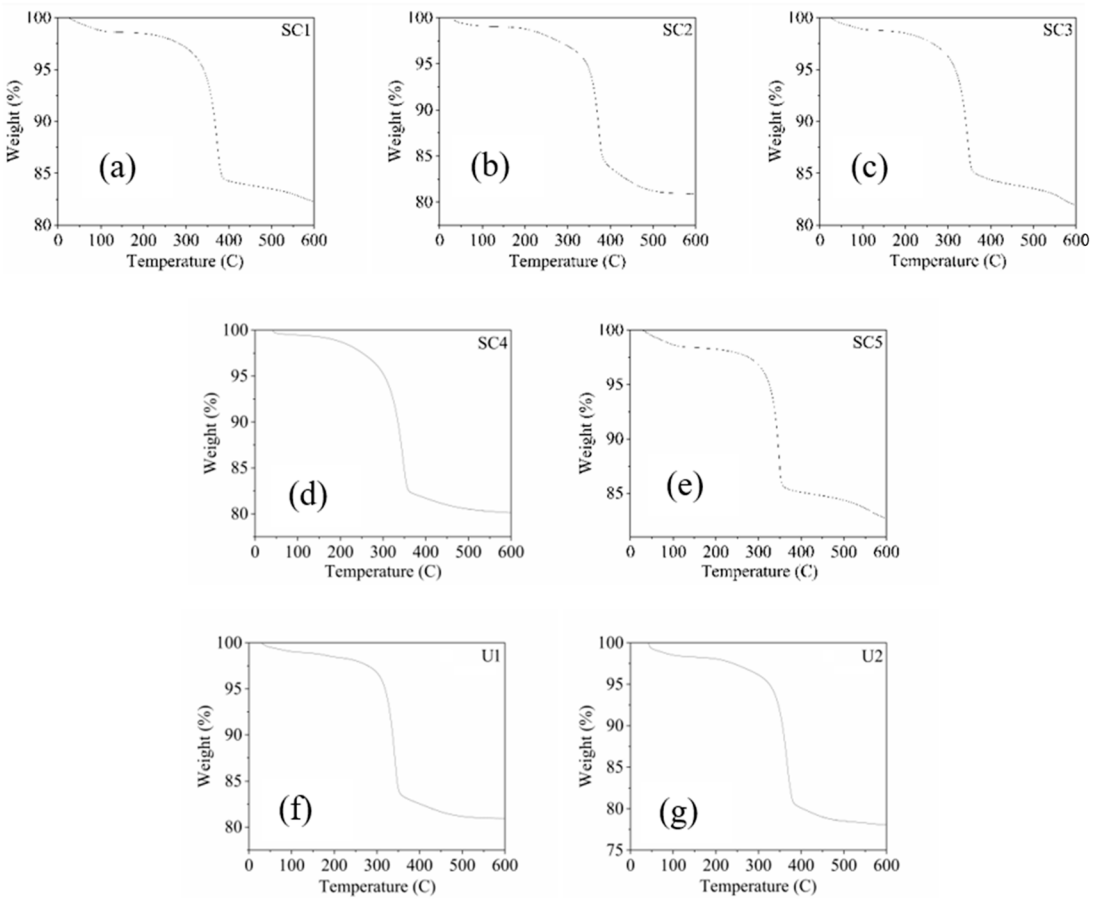

Figure 5. (**a**–**g**) TGA curves of supercapacitors for SC1–5, U1, and U2, respectively.

Across all samples, the TGA curves reveal a three-stage decomposition profile:

1. Initial weight loss below 150 °C is relatively minor and typically attributed to moisture desorption and evaporation of volatile surface contaminants.
2. Major decomposition occurs between ∼250 °C and 420 °C corresponding to the thermal degradation of organic binder materials such as PVDF or other polymer-based additives.
3. A secondary, slower degradation phase above 420 °C reflects the breakdown of more stable carbonaceous structures or residual ash-forming materials.

These thermal trends provide supporting evidence for material composition differences and structural integrity across the tested supercapacitors. The TGA results contribute to understanding how variations in electrode formulation impact long-term performance

and degradation resistance. From the TGA data, the following quantitative features were extracted and used as input for the machine learning models: DTG peak (%/°C), temperature corresponding to the DTG peak (°C), and remaining mass (%) at 600 °C. The collected material composition results are presented in Table 3. These detailed analyses provided deeper insights into the structural and compositional factors influencing the performance and degradation behavior of the commercial supercapacitors.

Table 3. Material composition of supercapacitors.

	Carbon (%)	Fluorine (%)	Porosity (%)	Particle Size (μm^2)	Remaining Weight (%)	Derivative Weight (mg/°C)	Derivative Temp. (°C)
SC1	91.5	8.5	9.23	1530.6	80.26	0.393	372
SC2	86.6	13.4	14.95	1434.2	80.87	0.4662	373
SC3	90.5	9.2	21.15	1879.2	81.9	0.3986	346
SC4	86.4	13.6	14.7	1073.7	80.13	0.376	346
SC5	90.3	9.7	13.8	1440	82.67	0.5081	347
U1	91.2	8.7	15.7	959.8	80.94	0.4948	342
U2	89.8	10.2	10.32	1090.5	78.09	0.464	366

3.3. CCCD Test Results: Effect of Voltage and Current on Capacity Retention

To evaluate the electrochemical stability and degradation behavior of commercial supercapacitors under different electrical conditions, three CCCD configurations were employed. The analysis was structured to isolate the effects of voltage and current individually on capacity retention.

3.3.1. Effect of Voltage: CCCD1 vs. CCCD2 (Constant Current = 5 A)

In the first comparison, the current was held constant at 5 A, while the voltage was increased from 2.6 V (CCCD1) to 3.5 V (CCCD2). This configuration aimed to assess how elevated voltage stress impacts long-term performance. The capacity retention curves for all five training samples (SC1–SC5) under CCCD1 and CCCD2 are shown side by side in Figure 6, highlighting the degradation patterns under both test conditions.

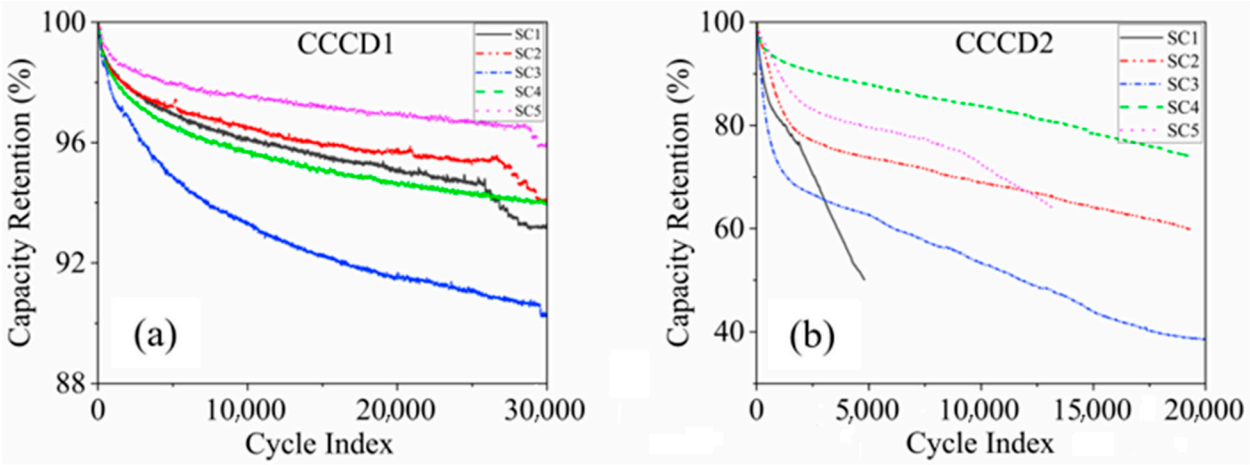

Figure 6. Capacity retention comparison under varying voltage at constant current (5 A) for training supercapacitors, (**a**): CCCD1, (**b**): CCCD2.

Under the lower voltage condition (CCCD1), most supercapacitors exhibited stable performance over 30,000 cycles, with SC5 retaining above 97% capacity. However, when the voltage was increased to 3.5 V (CCCD2), several samples experienced accelerated degradation. Notably, SC1 and SC3 dropped below 50% retention within the first 5000 cycles,

while SC4 and SC5 showed relatively higher resilience, maintaining above 75% and 85% capacity, respectively, by the end of 20,000 cycles.

The same comparison was performed for the unseen validation samples (U1 and U2), as shown in Figure 7. Consistent with the training set, both unseen samples displayed increased degradation at higher voltage. U1 retained approximately 65% of its capacity at the end of CCCD2, compared to over 85% in CCCD1. This confirms that voltage plays a significant role in accelerating failure mechanisms, such as electrolyte decomposition or electrode oxidation, across different device types.

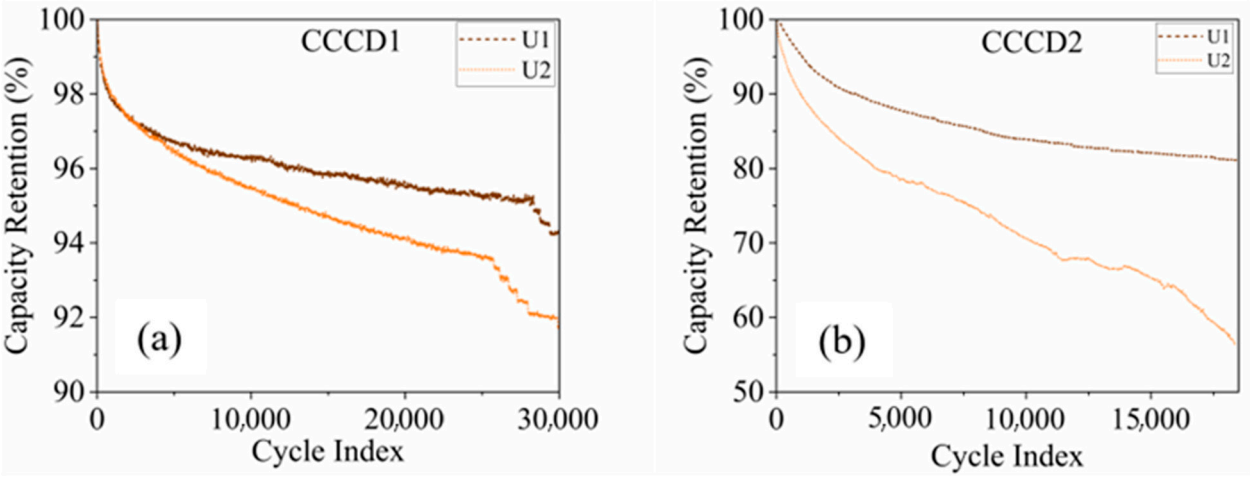

Figure 7. Capacity retention comparison under varying voltage at constant current (5 A) for unseen supercapacitors, (**a**): CCCD1, (**b**): CCCD2.

3.3.2. Effect of Current: CCCD2 vs. CCCD3 (Constant Voltage = 3.5 V)

In the second comparison, the voltage was fixed at 3.5 V, while the current was decreased from 5 A (CCCD2) to 3 A (CCCD3). This comparison was designed to study the effect of reduced current on degradation behavior. The capacity retention results for the training samples are shown in Figure 8.

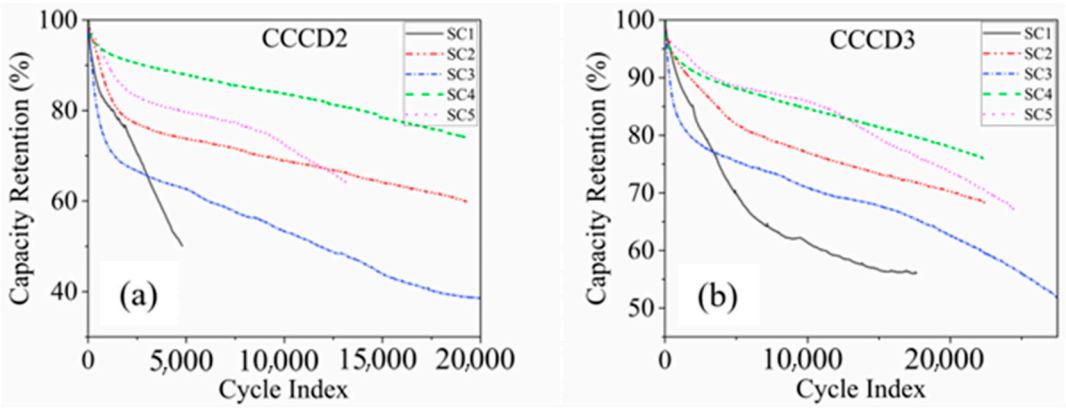

Figure 8. Capacity retention comparison under varying current at constant voltage (3.5 V) for training supercapacitors, (**a**): CCCD2, (**b**): CCCD3.

Reducing the current from 5 A to 3 A led to improved stability in most cases. SC4 and SC5 demonstrated the best performance under CCCD3, retaining above 85% capacity after 20,000 cycles. SC2 also showed moderate improvement. SC1 and SC3, which previously degraded rapidly under CCCD2, still experienced significant loss but at a slower rate under CCCD3, indicating that the current intensity has a direct effect on heat generation and mechanical strain during cycling.

The unseen supercapacitors exhibited similar trends, as shown in Figure 9. U1, for example, retained approximately 75% capacity under CCCD3, compared to just 65% under CCCD2. These results confirm that lowering the current while maintaining high voltage mitigates some degradation effects, particularly for devices more prone to thermal or electrochemical instability.

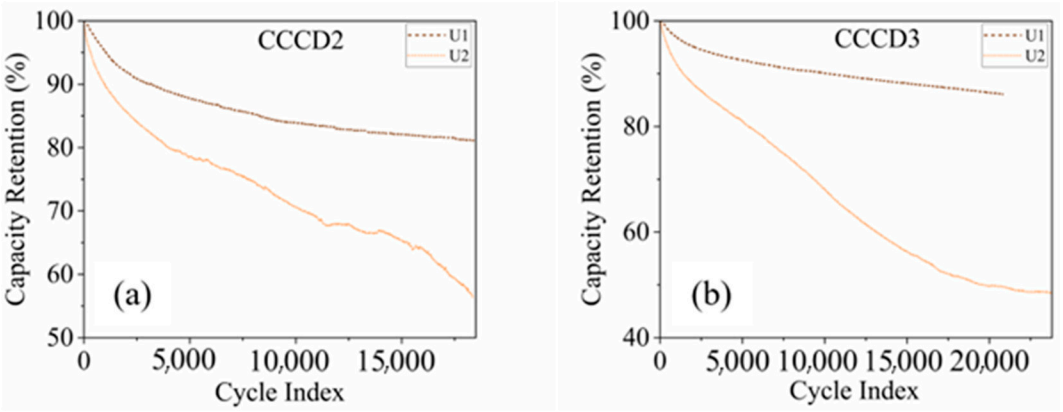

Figure 9. Capacity retention comparison under varying current at constant voltage (3.5 V) for unseen supercapacitors, (**a**): CCCD2, (**b**): CCCD3.

3.4. Correlating Capacity Retention with Structural and Material Properties

The variation in capacity retention observed across different CCCD tests can be partly attributed to the material composition, structural morphology, and physical dimensions of the tested supercapacitors. Supercapacitors that demonstrated higher stability under both voltage and current stress conditions, such as SC5 and SC4, also exhibited moderate porosity, balanced electrode mass, and favorable thermal and elemental characteristics, suggesting a strong link between physical/material properties and electrochemical resilience.

SEM analysis revealed that SC5, which retained over 85% of its capacity across all CCCD conditions, possessed a uniform and moderately porous electrode surface, with a porosity value of 13.8%. This optimized microstructure may have facilitated uniform ion distribution and reduced mechanical degradation during cycling. In contrast, SC3, which showed severe degradation (retaining only ~50% capacity under CCCD2 and CCCD3), had the highest porosity (21.15%) and the most irregular surface texture, likely leading to poor structural integrity and increased electrolyte penetration, accelerating capacity fade.

These findings highlight that higher porosity does not necessarily correlate with greater electrochemical stability. Excessive porosity may lead to non-uniform ion transport pathways, causing localized overcharging, uneven current distribution, and mechanical stress accumulation within the electrode structure. Therefore, an optimal range of porosity—not simply maximizing it—is critical for achieving balanced ion accessibility and structural robustness. EDS results also support this observation. SC1 and SC3, which degraded quickly under elevated voltage and current, had relatively lower carbon content and higher fluorine percentages compared to SC5 and SC4. Excess fluorine content, associated with PVDF binders, may increase mechanical rigidity but also reduce active surface area, contributing to early failure. On the other hand, SC5 maintained a balanced elemental profile, supporting better electron conduction and mechanical resilience.

From a thermal stability perspective, TGA results showed that SC5 and SC2 had the highest remaining weight percentages after thermal decomposition, indicating a higher content of thermally stable carbonaceous material. SC3, by contrast, exhibited a sharp mass loss at a lower temperature, suggesting the presence of more volatile or weakly bound compounds, which could contribute to its accelerated degradation during extended cycling.

Moreover, physical measurements offered further insight. SC4 and SC5 had electrodes with thinner profiles and lower weights, which may have facilitated better heat dissipation and lower mechanical strain during charge–discharge cycles. In contrast, SC2 and SC3 had thicker, heavier electrodes that might have contributed to localized thermal buildup and uneven stress distribution—conditions that can intensify material fatigue and electrolyte decomposition under high-voltage or high-current operations.

To investigate the broader relationship between thermal stability and electrochemical performance, we analyzed the trend between the TGA-derived remaining weight percentage at 600 °C and the capacity retention across all CCCD conditions. A consistent pattern was observed: supercapacitors with higher thermal residue tended to maintain greater capacity retention under both moderate (CCCD1) and elevated stress conditions (CCCD2 and CCCD3). For example, SC5, which exhibited the highest remaining mass (82.67%), consistently retained over 85% of its capacity in all three CCCD tests. In contrast, SC3, with a lower residue (81.9%), showed severe degradation, especially under high-voltage or high-current conditions. This suggests that greater thermal residue is indicative of more thermally stable and structurally resilient electrode materials, which are less prone to decomposition, delamination, or pore collapse during extended cycling. These findings reinforce the value of incorporating thermal stability metrics into predictive modeling frameworks for degradation, as they offer insight into long-term reliability under various electrical stresses.

In summary, the integration of morphological, compositional, thermal, and structural insights provides a clearer explanation of the diverse capacity retention behaviors observed in the cycler tests. Supercapacitors with moderate porosity, thermally stable materials, and optimized physical dimensions consistently outperformed others, validating the importance of combining electrical and material analyses in predictive modeling.

3.5. Training Models

3.5.1. Linear Regression

To evaluate the effectiveness and generalizability of Linear Regression in predicting capacity retention, the model was tested under two configurations:

- Using only cycler-derived features (test data).
- Using cycler + material features (test and unseen data).

The training dataset consisted of cycling results and material characterizations from five different commercial supercapacitors. The data were merged by sample ID and stratified by supercapacitor type to ensure balanced sampling across the classes. Feature values were standardized using Standard Scaler, and models were trained using a 70/30 train-test split. The results are summarized in Figure 10, which presents performance metrics and error distributions for both test and unseen datasets.

In the test dataset, adding material features to the cycler data led to a clear improvement in model accuracy. The R^2 value increased from 0.88 to 0.955, while MAE and RMSE dropped from 3.93% to 2.49% and 5.08% to 3.12%, respectively. This indicates that incorporating material and physical properties helps the model capture additional degradation-related information not present in electrical data alone.

Importantly, the inclusion of material features also improved prediction robustness on unseen data. While the model trained on cycler-only features struggled to generalize beyond the training set, adding material inputs yielded an R^2 of 0.917 and maintained a low MAE of 2.76% and RMSE of 3.74%. These results highlight the positive contribution of intrinsic material characteristics, such as porosity, electrode composition, and thermal stability, to predictive generalization.

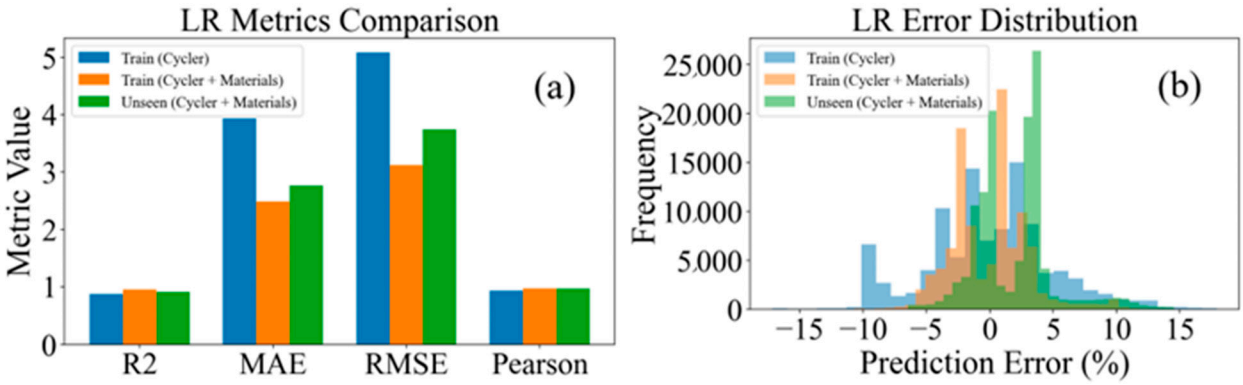

Figure 10. Performance metrics and error distributions for Linear Regression model, (**a**): performance comparison for all data, (**b**): error distribution for all data.

The error distributions further support these observations. As seen in Figure 10 (bottom row), the cycler-only model exhibits wider error spreads with multiple large deviations, particularly on unseen samples. In contrast, the inclusion of material features yields tighter, more symmetric error distributions, suggesting not only better model fit but also improved consistency when predicting new, untested devices.

Table 4 presents a quantitative summary of the Linear Regression model's performance across three scenarios: using only cycler data (Train Cycler), using combined cycler and material features (Train Cycler + Material), and evaluating the trained model on unseen supercapacitors (Unseen Cycler + Material). As shown, the inclusion of material features substantially improved all performance metrics during training, with R^2 rising from 0.879 to 0.955, and MAE and RMSE dropping to 2.49% and 3.12%, respectively. Notably, the model maintained high accuracy even on unseen data, achieving an R^2 of 0.917 and a Pearson correlation of 0.971, confirming the material features' contribution to enhanced generalization. These results validate the value of integrating structural and compositional properties into predictive frameworks, even within a simple linear modeling approach.

Table 4. LR performance comparison for all data.

	Feature Set	R^2	MAE	RMSE	Pearson
Train	Cycler	0.879487	3.934272	5.079233	0.94
Train	Cycler + Material	0.954541	2.486132	3.119533	0.98
Unseen	Cycler + Material	0.916906	2.762770	3.740433	0.971110

3.5.2. Random Forest

To further investigate the predictive capability of classical ensemble methods, a Random Forest Regressor was developed to estimate the capacity retention of commercial supercapacitors. To mitigate overfitting and enhance generalization, hyperparameter tuning was conducted using GridSearchCV with 5-fold cross-validation. The parameter grid included constraints such as limiting the number of estimators (n_estimators = 100, 200), setting maximum tree depth (max_depth = 10 or 20), and enforcing a minimum number of samples per leaf node (min_samples_leaf = 100, 300). Additionally, the max_features parameter was tuned (sqrt and 0.5) to reduce input dimensionality per split. These regularization strategies were selected to balance model flexibility with robustness, particularly in scenarios involving a high-dimensional input space due to material features. Despite this, the model showed signs of overfitting when tested on unseen data, indicating that further techniques such as feature selection or model ensemble averaging may be necessary in future work. As shown in Figure 11a, incorporating material features significantly

improved performance on the test dataset. The R^2 increased from 0.63 to 0.84, and both MAE and RMSE decreased from 5.93% to 3.89% and from 9.56% to 6.30%, respectively. These improvements suggest that Random Forest effectively leveraged material inputs such as porosity, electrode thickness, and thermal degradation profiles to capture nonlinear relationships influencing degradation behavior.

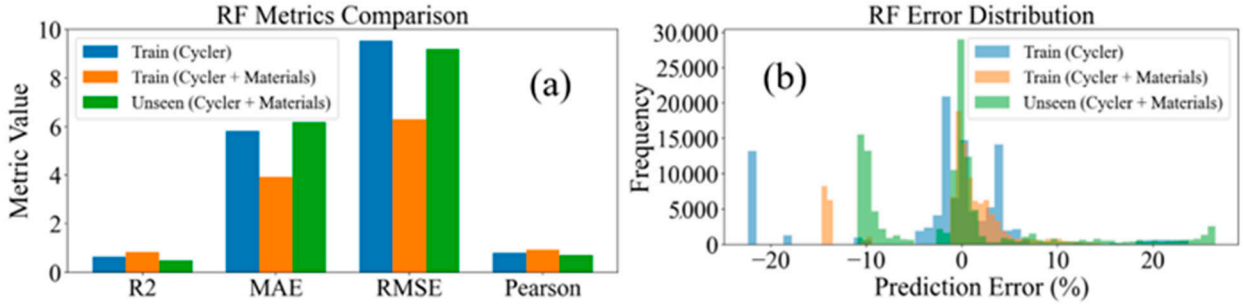

Figure 11. Performance metrics and error distributions for Random Forest model, (**a**): performance comparison for all data, (**b**): error distribution for all data.

However, this benefit did not fully translate to the unseen dataset. When evaluated on supercapacitors not included in training, the model trained with cycler + material features experienced a drop in performance, with R^2 decreasing to 0.48 and RMSE increasing to 9.34%, nearly reverting to cycler-only levels. This decline suggests that while material features helped the model fit the training distribution more accurately, they may have also introduced overfitting or dataset-specific noise that hindered generalization.

The error distributions in Figure 11b reinforce this observation. For the test data, adding material features clearly narrowed the error spread and centered it around zero, indicating better accuracy and reduced variance. In contrast, the unseen data error distribution showed wider tails and more outliers, highlighting the model's reduced stability when applied to new samples. These findings point to Random Forest's sensitivity to feature noise and suggest that additional regularization or feature selection may be needed to improve robustness.

Table 5 presents the quantitative performance metrics of the Random Forest model across three scenarios: training with only cycler features, training with cycler + material features, and evaluation of unseen supercapacitors using the cycler + material model. When trained on cycler-only features, the model achieved a modest performance with an R^2 of 0.633 and a relatively high RMSE of 9.56%, indicating limited capacity to capture the degradation behavior using cycling data alone.

Table 5. RF performance comparison for all data.

	Feature Set	R^2	MAE	RMSE	Pearson
Train	Cycler	0.633	5.933	9.558	0.805
Train	Cycler + Material	0.841	3.894	6.300	0.920
Unseen	Cycler + Material	0.482	6.285	9.336	0.695

Incorporating material features during training substantially improved predictive power, raising the R^2 to 0.841 and reducing RMSE to 6.30%. This demonstrates that Random Forest effectively utilized material-level inputs such as porosity, electrode thickness, and thermal properties to capture complex degradation mechanisms. Furthermore, the Pearson correlation increased significantly to 0.920, reinforcing the model's ability to align well with true capacity retention trends.

However, on the unseen validation dataset, performance dropped noticeably. The R^2 declined to 0.482 and RMSE increased to 9.34%, which is comparable to the cycler-only model. Although the test data showed strong predictive accuracy, this decline on unseen samples suggests potential overfitting to training patterns or dataset-specific material characteristics. The decrease in Pearson correlation to 0.695 further highlights a loss in generalization. These results suggest that while material features boost learning on known data, additional regularization or broader training diversity may be necessary to enhance robustness across new supercapacitor types.

3.5.3. MLP (Multi-Layer Perceptron)

To explore the effectiveness of deep learning in modeling supercapacitor degradation, a Multi-Layer Perceptron (MLP) Regressor was employed. MLP is a type of feedforward artificial neural network capable of capturing complex nonlinear relationships through its hidden layers. Two models were trained: one using only cycling features and another using an augmented feature set that included selected material properties and engineered interaction terms. Feature engineering involved the creation of nonlinear interaction variables such as Current × Voltage and Charge Time × Discharge Time, enhancing the model's capacity to learn meaningful patterns. As shown in Figure 12, the inclusion of material inputs significantly enhanced the model's learning capacity and predictive accuracy.

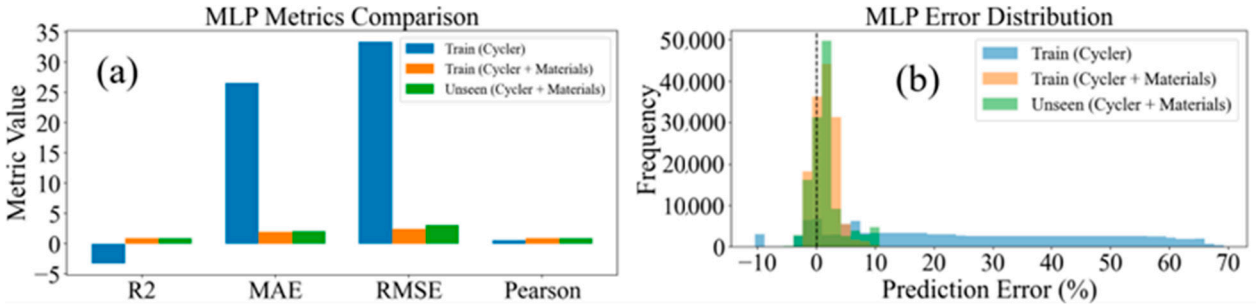

Figure 12. Performance metrics and error distributions for MLP model, (**a**): performance comparison for all data, (**b**): error distribution for all data.

On the training dataset, the model trained with cycler-only features performed poorly, exhibiting a negative R^2 of −3.26, an MAE of 26.6%, and an RMSE of over 33.4%—worse than a baseline mean predictor. After incorporating material and physical features, however, the model's performance improved dramatically, achieving an R^2 of 0.976, MAE of 1.97%, and RMSE of 2.50%. This indicates that MLP relies heavily on the nonlinear and complementary nature of material descriptors to learn degradation behavior effectively.

The error distribution plots in Figure 12b further illustrate this transformation. The cycler-only model produced a broad, skewed error profile with extreme deviations exceeding 60%. In contrast, the cycler + material configuration yielded a narrow, symmetric distribution centered near zero, demonstrating improved stability and accuracy.

Despite being trained only on known samples, the MLP model also performed well on unseen data, as indicated in Table 6. While some increase in error was expected, the model maintained a high R^2 of 0.941 and RMSE of 3.15%, indicating that the incorporated material features improved generalization. The corresponding errors with the histogram for unseen data (Figure 12b) remained compact, with most predictions within a ±3% range. This shows that the MLP not only captured complex patterns during training but also generalized well when supported by carefully selected structural and material attributes.

Table 6. Metrics performance for MLP in train and unseen data.

	Feature Set	R^2	MAE	RMSE	Pearson
Train	Cycler	−3.255	26.58	33.408	0.575
Train	Cycler + Material	0.976	1.967	2.497	0.994
Unseen	Cycler + Material	0.941	2.142	3.145	0.994

A comprehensive comparison of model performance across three machine learning algorithms Linear Regression, Random Forest, and MLP (Multi-Layer Perceptron) under three scenarios: training with cycler features only, training with cycler plus material features, and evaluation on unseen data using cycler plus material features, is presented in Table 7. The performance is assessed using four key metrics: R^2, MAE, RMSE, and Pearson correlation. The superior performance of the MLP model can be attributed to its deep nonlinear learning capability and ability to automatically capture complex feature interactions. Unlike linear models that assume additive relationships or tree-based models that rely on axis-aligned splits, MLPs utilize multiple hidden layers and activation functions to learn nonlinear transformations of the input space. This is especially advantageous in this study, where temporal degradation behavior, structural parameters, and material features interact in nontrivial ways. For instance, the effect of porosity may depend on electrode thickness or cycling voltage interactions that are naturally learned by neural networks. Additionally, the inclusion of engineered features (e.g., Current × Voltage, Charge Time × Discharge Time) further enhanced the model's ability to generalize by enriching the representation space. These characteristics make MLPs well-suited for predicting supercapacitor degradation, where both linear trends and subtle multivariate patterns co-exist.

Table 7. Performance comparison for different ML models under different scenarios. Green cells indicate the best performance values for each metric.

Model	Train Cycler Only				Train Cycler + Material				Unseen Cycler + Material			
	R^2	MAE	RMSE	Pearson	R^2	MAE	RMSE	Pearson	R^2	MAE	RMSE	Pearson
LR	0.879	3.934	5.079	0.938	0.955	2.486	3.120	0.977	0.917	2.763	3.740	0.971
RF	0.633	5.933	9.558	0.805	0.841	3.894	6.300	0.920	0.482	6.285	9.336	0.695
MLP	−3.26	26.58	33.41	0.575	0.976	1.968	2.497	0.994	0.941	2.147	3.145	0.994

Across all three models, the addition of material features consistently enhances model performance. For instance, in the Linear Regression model, the R^2 increased from 0.879 (cycler only) to 0.955 (cycler + materials), and MAE dropped from 3.93 to 2.49, demonstrating the value of including electrochemical and physical material descriptors. A similar trend is seen in the Random Forest model, where R^2 improved from 0.633 to 0.841 and MAE dropped from 5.93 to 3.89 upon adding material features.

The MLP model benefited the most from the inclusion of material features. Without them, it failed to generalize and exhibited poor performance ($R^2 = -3.26$, RMSE = 33.41), but once material features were included, it achieved the best overall results, with an R^2 of 0.976, MAE of 1.97, and RMSE of 2.49 on the training set. Even on unseen data, the MLP retained strong predictive performance ($R^2 = 0.941$, Pearson = 0.994).

To evaluate the contribution of material and physical features to the capacity retention prediction, we analyzed feature importance rankings for all three models: Linear Regression, Random Forest, and Multilayer Perceptron (MLP). While electrical parameters such as voltage and current consistently emerged as dominant predictors, several material and physical features also demonstrated significant influence. Specifically, features such as

electrode weight, density, thickness, and Fluorine percentage appeared prominently in the Random Forest and MLP models, highlighting their relevance to the degradation behavior of supercapacitors. Additionally, the Linear Regression model assigned meaningful coefficients to features like remaining weight in the TGA test, DTG temperature, and derivative weight, indicating that thermal and compositional properties affect long-term performance. These findings underscore the complementary role of material characterization data in enhancing model interpretability and predictive accuracy beyond conventional electrical metrics. The detailed visualization of feature importance for each model is provided in Supplementary Materials (Figure S5).

In summary, this analysis underscores the critical role of material features in improving model performance for capacity retention prediction. Across all three machine learning models—Linear Regression, Random Forest, and MLP—the inclusion of material descriptors led to consistent and often substantial enhancements in accuracy. These descriptors, which include properties such as electrode thickness, porosity, and thermal degradation behavior, provide essential physical and structural context that cycling data alone cannot capture. Their presence enables models to better understand and predict the long-term electrochemical behavior of supercapacitors.

While Linear Regression showed improved performance with material inputs, the effect was most pronounced in more complex models. For Random Forest, material features reduced prediction error on the test set by a wide margin, though challenges in generalization remained. In contrast, the MLP model, which initially struggled with cycler-only features, exhibited exceptional performance once material features were included, achieving the best results across all metrics, both in training and on unseen data. This indicates that neural networks, with their ability to model nonlinear relationships, are particularly well-suited to harness the predictive power of diverse material attributes.

Overall, these findings highlight that material features are not merely supplementary but essential for accurate and robust modeling of supercapacitor degradation. Their integration transforms simple data-driven models into more physically informed predictive tools, enabling better generalization across different device chemistries and operational histories. As such, future work on predictive modeling in energy storage should prioritize the systematic collection, selection, and integration of material-level data to maximize both model performance and reliability.

In addition to the discussion, it should be noted that the machine learning-based approach presented in this study is applicable not only to commercial supercapacitors but also to non-commercial ones, including those fabricated in laboratory environments. As demonstrated in a study by the same authors (Khosravinia et al., iScience 2023) [23], a similar framework was successfully applied to predict the performance of pseudo-capacitors produced using ultra-short laser pulses for direct electrode fabrication. This supports the generalizability of the approach across a wide range of supercapacitor systems, irrespective of their commercial status.

4. Conclusions

In this study, a comprehensive framework was developed to predict the capacity retention of commercial supercapacitors using machine learning models informed by both electrical cycling data and experimentally derived material and structural features. By integrating extensive lab-generated charge–discharge data with physical measurements (e.g., electrode dimensions, weight) and material characterizations (SEM, EDS, TGA), we created a multimodal dataset that captures both the operational and intrinsic properties influencing degradation.

Three machine learning models, Linear Regression (LR), Random Forest (RF), and Multi-Layer Perceptron (MLP), were trained and evaluated under multiple scenarios to assess the predictive value of material features. Across all models, the inclusion of material descriptors led to a substantial improvement in performance. Notably, the MLP model achieved the highest accuracy, with an R^2 of 0.976 on the training set and 0.941 on unseen data, confirming its ability to capture complex nonlinear relationships between material properties and electrochemical degradation behavior. Even simpler models like LR demonstrated improved generalizability when augmented with material features, achieving an R^2 of 0.917 on unseen data.

The results highlight the essential role of material-level information such as porosity, elemental composition, electrode thickness, and thermal stability in accurately modeling supercapacitor degradation. These features provided critical context that complemented electrical parameters and significantly enhanced model interpretability and robustness. Importantly, this study demonstrates that meaningful insights into device aging and reliability can be achieved not only through electrical testing but also through detailed material analysis, offering a more holistic understanding of supercapacitor behavior.

Overall, this work demonstrates that combining experimental material data with machine learning is a powerful and practical approach for capacity retention prediction. The findings provide a valuable direction for designing more accurate and physically informed predictive models in the domain of energy storage system assessment.

Looking ahead, several future directions can extend the impact of this work. One promising avenue is the development of early-cycle prediction models, where initial charge–discharge behavior is used to forecast long-term capacity retention. This approach could greatly reduce testing time and accelerate the screening of commercial and lab-fabricated supercapacitors. Additionally, expanding the dataset to include diverse supercapacitor chemistries and form factors would also support the application of transfer learning across different technologies.

Supplementary Materials: The following supporting information can be downloaded at: https://www.mdpi.com/article/10.3390/batteries11070264/s1, Figure S1: Sixth-Order Polynomial Fit of Capacity Retention for SC1 under CCCD1 Conditions, Figure S2: Battery cycler parameters PC settings for CCCD2, Figure S3: Threshold Segmentation in ImageJ for Porosity Analysis, Figure S4: EDS Layered Images for all supercapacitors, Figure S5: Feature importance for all Machine Learning Models (a): Linear Regression, (b): Random Forest, (c): MLP; Table S1: Summary of CCCD Test Protocols Parameters Used in Supercapacitor Cycling;. Supplementary Information includes additional Feature importance for all Machine Learning Models.

Author Contributions: M.K.K.: writing—original draft, methodology, investigation, formal analysis, data curation. K.K.: methodology, formal analysis, data curation, writing—review and editing. A.K.: conceptualization, methodology, supervision, validation, resources, project administration, funding acquisition, writing—review and editing. All authors have read and agreed to the published version of the manuscript.

Funding: This work was supported by the Natural Sciences and Engineering Research Council of Canada (NSERC) (grant number: RGPIN-2022-03992).

Data Availability Statement: The data that support the findings of this study are included within the article. Raw data can be requested from the author (the raw data will be made available upon reasonable request on a case-by-case basis. State that this is due to our IP agreement with our industrial partner and our ongoing IP generation and optimization projects using this data). Additional data can also be found in the Supplementary Materials.

Conflicts of Interest: The authors declare the following potential competing interests: Amirkianoosh Kiani reports financial support from the Natural Sciences and Engineering Research Council of

Canada. The other authors declare no known competing financial interests or personal relationships that could have influenced the work reported in this paper.

References

1. Zhang, L.L.; Zhao, X.S. Carbon-based materials as supercapacitor electrodes. *Chem. Soc. Rev.* **2009**, *38*, 2520–2531. [CrossRef] [PubMed]
2. Libich, J.; Máca, J.; Vondrák, J.; Čech, O.; Sedlaříková, M. Supercapacitors: Properties and applications. *J. Energy Storage* **2018**, *17*, 224–227. [CrossRef]
3. González, A.; Goikolea, E.; Barrena, J.A.; Mysyk, R. Review on supercapacitors: Technologies and materials. *Renew. Sustain. Energy Rev.* **2016**, *58*, 1189–1206. [CrossRef]
4. Saikia, B.K.; Benoy, S.M.; Bora, M.; Tamuly, J.; Pandey, M.; Bhattacharya, D. A brief review on supercapacitor energy storage devices and utilization of natural carbon resources as their electrode materials. *Fuel* **2020**, *282*, 118796. [CrossRef]
5. Sharma, P.; Kumar, V. Study of electrode and electrolyte material of supercapacitor. *Mater. Today Proc.* **2020**, *33*, 1573–1578. [CrossRef]
6. Miller, E.E.; Hua, Y.; Tezel, F.H. Materials for energy storage: Review of electrode materials and methods of increasing capacitance for supercapacitors. *J. Energy Storage* **2018**, *20*, 30–40. [CrossRef]
7. Yang, H. A comparative study of supercapacitor capacitance characterization methods. *J. Energy Storage* **2020**, *29*, 101316. [CrossRef]
8. Lobato, B.; Suárez, L.; Guardia, L.; Centeno, T.A. Capacitance and surface of carbons in supercapacitors. *Carbon* **2017**, *122*, 434–445. [CrossRef]
9. Patel, A.; Patel, S.K.; Singh, R.S.; Patel, R.P. Review on recent advancements in the role of electrolytes and electrode materials on supercapacitor performances. *Discov. Nano* **2024**, *19*, 188. [CrossRef]
10. El Mejdoubi, A.; Chaoui, H.; Sabor, J.; Gualous, H. Remaining useful life prognosis of supercapacitors under temperature and voltage aging conditions. *IEEE Trans. Ind. Electron.* **2017**, *65*, 4357–4367. [CrossRef]
11. Ortega, P.F.R.; Trigueiro, J.P.C.; Silva, G.G.; Lavall, R.L. Improving supercapacitor capacitance by using a novel gel nanocomposite polymer electrolyte based on nanostructured SiO_2, PVDF and imidazolium ionic liquid. *Electrochim. Acta* **2016**, *188*, 809–817. [CrossRef]
12. Zhang, Y.-Z.; Cheng, T.; Wang, Y.; Lai, W.-Y.; Pang, H.; Huang, W. A simple approach to boost capacitance: Flexible supercapacitors based on manganese oxides@ MOFs via chemically induced in situ self-transformation. *Adv. Mater.* **2016**, *28*, 5242–5248. [CrossRef]
13. Nguyen, N.T.; Ozkan, S.; Hwang, I.; Zhou, X.; Schmuki, P. Spaced TiO_2 nanotube arrays allow for a high performance hierarchical supercapacitor structure. *J. Mater. Chem. A* **2017**, *5*, 1895–1901. [CrossRef]
14. Zhu, S.; Li, J.; Ma, L.; He, C.; Liu, E.; He, F.; Shi, C.; Zhao, N. Artificial neural network enabled capacitance prediction for carbon-based supercapacitors. *Mater. Lett.* **2018**, *233*, 294–297. [CrossRef]
15. Reddy, B.S.; Narayana, P.L.; Maurya, A.K.; Paturi, U.M.R.; Sung, J.; Ahn, H.-J.; Cho, K.K.; Reddy, N.S. Modeling capacitance of carbon-based supercapacitors by artificial neural networks. *J. Energy Storage* **2023**, *72*, 108537. [CrossRef]
16. Komarsofla, A.K.; Charest-Finn, M.; Nokleby, S. Autonomous Inspection of Steel Pipe Weld Lines Implementing Frequency Analysis Combined with YOLOv5. In Proceedings of the Canadian Society for Mechanical Engineering International Congress 2023, Sherbrooke, QC, Canada, 28–31 May 2023.
17. Tawfik, W.Z.; Mohammad, S.N.; Rahouma, K.H.; Tammam, E.; Salama, G.M. An artificial neural network model for capacitance prediction of porous carbon-based supercapacitor electrodes. *J. Energy Storage* **2023**, *73*, 108830. [CrossRef]
18. Ren, J.; Lin, X.; Liu, J.; Han, T.; Wang, Z.; Zhang, H.; Li, J. Engineering early prediction of supercapacitors' cycle life using neural networks. *Mater. Today Energy* **2020**, *18*, 100537. [CrossRef]
19. Komarsofla, M.K.; Singh, H.; Kiani, A. Data-Driven Approaches for Predicting Supercapacitor Degradation Behaviour. In Proceedings of the 247th ECS Meeting, Montréal, QC, Canada, 18–22 May 2025; ECS: Pennington, NJ, USA, 2025.
20. Wei, L.; Wang, Y.; Lin, T.; Huang, X.; Yan, R. Life prediction of on-board supercapacitor energy storage system based on gate recurrent unit neural network using sparse monitoring data. *Appl. Energy* **2025**, *379*, 124917. [CrossRef]
21. Khosravinia, K.; Kiani, A. Unlocking pseudocapacitors prolonged electrode fabrication via ultra-short laser pulses and machine learning. *Iscience* **2023**, *26*, 106438. [CrossRef]
22. Khosravinia, K.; Kiani, A. AI-Driven Laser Parameter Optimization for Enhanced Pseudocapacitor Electrodes. In *CLEO: Applications and Technology*; Optica Publishing Group: Washington, DC, USA, 2024; p. JTu2A–1.
23. Mishra, S.; Srivastava, R.; Muhammad, A.; Amit, A.; Chiavazzo, E.; Fasano, M.; Asinari, P. The impact of physicochemical features of carbon electrodes on the capacitive performance of supercapacitors: A machine learning approach. *Sci. Rep.* **2023**, *13*, 6494. [CrossRef]
24. Su, H.; Lin, S.; Deng, S.; Lian, C.; Shang, Y.; Liu, H. Predicting the capacitance of carbon-based electric double layer capacitors by machine learning. *Nanoscale Adv.* **2019**, *1*, 2162–2166. [CrossRef] [PubMed]

25. Adekoya, G.J.; Adekoya, O.C.; Ugo, U.K.; Sadiku, E.R.; Hamam, Y.; Ray, S.S. A mini-review of artificial intelligence techniques for predicting the performance of supercapacitors. *Mater. Today Proc.* **2022**, *62*, S184–S188. [CrossRef]
26. Hastie, T.; Tibshirani, R.; Friedman, J. *The Elements of Statistical Learning*; Springer: New York, NY, USA, 2009.
27. Goodfellow, I.; Bengio, Y.; Courville, A.; Bengio, Y. *Deep Learning*; MIT Press: Cambridge, MA, USA, 2016; Volume 1, no. 2.